Proceedings of the Canadian Society for Mechanical Engineering International Congress
32nd Annual Conference of the Computational Fluid Dynamics Society of Canada
Canadian Society of Rheology Symposium
CSME-CFDSC-CSR 2025
May 25–28, 2025, Montréal, Québec, Canada

EXPERIMENTAL TESTING OF FOUR DIFFERENT ACTIVE VIBRATION CONTROLLERS ON A CLAMPED SANDWICH BEAM WITH NONLINEAR VIBRATIONS

Celia Hameury[1*], Giovanni Ferrari[2], Marco Amabili[1,3]
[1]Mechanical Engineering, McGill University, Montréal, Canada
[2]École de technologie supérieure, Université de Québec, Montréal, Canada
[3]School of Engineering, Westlake University, Hangzhou, China
*celia.hameury@mail.mcgill.ca

Abstract— Nonlinear vibration control is an area of growing interest in engineering. Geometric nonlinearities arise when vibration amplitudes become too large. While nonlinear vibrations have been controlled in the past, studies have never considered more than the first mode of vibration. This work aims to develop a novel dual-mode multi-input multi-output (MIMO) positive position feedback (PPF) controller. This controller was designed with two linear PPF filters, targeting the first and second natural modes, each in parallel with a cubic stiffness term. The controller was designed using SIMULINK and applied using piezoelectric actuator and sensor patches on a clamped sandwich beam, exhibiting hardening behaviour when excited by a stepped-sine excitation with increasing forcing levels. It was then compared to four other controllers: a SISO controller, a linear MIMO controller and two single-mode MIMO controllers, targeting the first and second modes respectively. The dual-mode MIMO PPF was shown to outperform the other four controllers in the control of the first two modes of vibration of the beam, making it the preferred option for such a purpose.

Keywords-component; active vibration control; nonlinear control; nonlinear vibrations; PPF; softening system.

I. INTRODUCTION

Nonlinear vibrations can arise due to numerous causes, including geometric nonlinearities, which occur when vibration amplitudes become fairly large [1, 2]. Geometric nonlinearities can result in two different nonlinear behaviours: (1) hardening behaviour, in which the structure's stiffness increases with increased forcing and (2) softening behaviour, in which the structure's stiffness decreases with increased forcing levels [3, 4]. Like linear vibrations, nonlinear ones can be dangerous for structures, and therefore must be appropriately controlled.

Active vibration control (AVC) was developed to mitigate large amplitude vibrations with low frequencies, which are difficult to damp using passive methods [5]. A popular AVC algorithm is positive position feedback (PPF), a second-order low-pass filter, developed by Caughey [6] and implemented experimentally by Fanson [7]. PPF is easy to implement with piezoelectric transducers, commonly used in the AVC field. Although designed for linear vibrations, PPF has been used to successfully reduce nonlinear vibrations as well. However, since PPF is designed to target only a single frequency of vibration, it loses effectiveness as the natural frequency of a nonlinear system shifts under increasing external function [8]. As a result, modifications have been attempted to make PPF-based controllers more suitable for nonlinear vibration control. Mahmoodi and Ahmandian attempted a modified PPF (MPPF) with an added first-order filter in [9]. This controller was successful, despite still being linear. Zhao et al. introduced a nonlinear cubic term to the linear PPF, designed to better target the nonlinearities of Duffing oscillator-type systems [10]. This controller was shown to outperform a linear one on a hardening cantilever beam. Hameury et al. also introduced a MIMO nonlinear PPF with a cubic term in [11, 12], which was tested experimentally on a hardening fixed beam presenting hardening geometric nonlinearities. This too was shown to outperform the linear version. The present work reiterates and synthesizes these findings comparing the novel controller by Hameury et al. to several other variations.

II. MATHEMATICAL MODELLING

A. System modelling

A system with hardening nonlinear behaviour, subject to a harmonic external force can be modelled as a Duffing oscillator:

$$\boldsymbol{M\ddot{x} + C\dot{x} + Kx + K_3x^3} = \boldsymbol{F_0}\cos(\omega t). \quad (1)$$

In the equation above, $\boldsymbol{M}$, $\boldsymbol{C}$, $\boldsymbol{K}$ and $\boldsymbol{K_3}$ are the mass, damping and stiffness matrices, all $n \times n$ in dimension, where n is the chosen number of degrees-of-freedom (DOF) of the system. $\boldsymbol{F_0}$ is the vector of forcing amplitudes, with dimensions $n \times 1$. The expression can be converted into the modal space, using the $n \times n$ modal matrix $\boldsymbol{\Phi}$ which has the property $\boldsymbol{\Phi}^T \boldsymbol{M} \boldsymbol{\Phi} = 1$. the effects of the sensors and actuators can be included as well, to obtain:

$$\ddot{\boldsymbol{q}} + 2\mathbf{Z}\boldsymbol{\Omega_n}\dot{\boldsymbol{q}} + [\Omega_n]^2\boldsymbol{q} + \boldsymbol{\eta_3}\boldsymbol{q^3} = \overline{\boldsymbol{F_0}}\cos(\omega t) + \overline{\boldsymbol{B_a}}\boldsymbol{V_a}, \quad (2)$$

$$\boldsymbol{V_s} = \overline{\boldsymbol{C_s}}\boldsymbol{q}. \quad (3)$$

Here, $\boldsymbol{\Omega_n}$ is the $n \times n$ diagonal matrix of natural frequencies, ω_n, and $\mathbf{Z_f}$ is the diagonal matrix of structure damping ratios, ζ. Then, q is the modal coordinate vector, with dimensions $n \times 1$. The matrices $\overline{\boldsymbol{B_a}}$ and $\overline{\boldsymbol{C_s}}$ are electromechanical coupling matrices, of dimensions $n \times m$ and $m \times n$ respectively, where m is the number of actuator-sensor pairs. The $\overline{\boldsymbol{B_a}}$ matrix converts the actuator voltage into modal forces while the $\overline{\boldsymbol{C_s}}$ matrix converts modal coordinates into sensor voltages.

B. Controller modelling

A controller is then added to the system, with a block diagram as shown in Fig. 1 below.

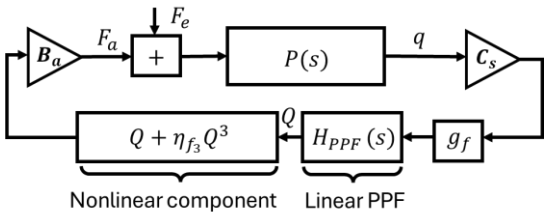

Figure 1. Block diagram of a nonlinaer PPF controller.

Using this diagram and the expressions in (2) and (3), the controller and system can now be written as,

$$\ddot{\boldsymbol{q}} + 2\mathbf{Z}\boldsymbol{\Omega_n}\dot{\boldsymbol{q}} + [\Omega_n]^2\boldsymbol{q} + \boldsymbol{\eta_3}\boldsymbol{q^3} = \overline{\boldsymbol{F_0}}\cos(\omega t) + \overline{\boldsymbol{B_a}}\,\boldsymbol{B_a^*}\left(\boldsymbol{Q} + \boldsymbol{\eta_{f_3}}\boldsymbol{Q^2}\right), \quad (4)$$

$$\ddot{\boldsymbol{Q}} + 2\mathbf{Z_f}\boldsymbol{\Omega_f}\dot{\boldsymbol{Q}} + \left[\Omega_f\right]^2\boldsymbol{Q} = \boldsymbol{g_f}\left[\Omega_f\right]^2\boldsymbol{C_s^*}\overline{\boldsymbol{C_s}}\boldsymbol{q}. \quad (5)$$

Here, $\boldsymbol{\Omega_f}$ is the matrix of controller frequencies, ω_f, and $\mathbf{Z_f}$ is the matrix of controller damping ratios, ζ_f. The term $\boldsymbol{g_f}$ denotes the matrix of controller gains, g_f. Matrices $\boldsymbol{B_a^*}$ and $\boldsymbol{C_s^*}$ are the inverses of the electromechanical matrices previously described, dubbed the controller matrices. They convert controller output into actuation voltages and sensor voltages into controller input respectively. They have dimensions $m \times n$ and $n \times m$ respectively. These must be chosen by the control designer. The values chosen for these terms for the novel dual-mode nonlinear MIMO PPF controller are presented in Table I, below. The controller frequencies were set equal to the structure's first two natural modes, while the damping ratios were chosen based on literature. The electromechanical coupling matrices were obtained using optimization techniques.

TABLE I. CONTROL PARAMETERS

Parameter	Mode 1 value	Mode 2 value
ω_f	64	158
ζ_f	0.3	0.3
g_f	0.3	0.5
η_{f_3}	0.1	0.2
$\boldsymbol{B_a^*}$	$\begin{bmatrix}-0.14\\0.14\end{bmatrix}$	$\begin{bmatrix}0.8069\\1.2153\end{bmatrix}$
$\boldsymbol{C_s^*}$	$[1.2079 \quad 9.5550]$	$[-0.3123 \quad 0.5964]$

III. EXPERIMENTAL METHODS

A. Experimental set-up

The experimental set-up used for this study was a composite sandwich beam with a PN2-1/8-3.0 PLASCORE® aramid honeycomb core and two layers of carbon-epoxy on either side. The beam was clamped to an aluminium frame on either end, with a length of 517 mm between the clamps. Its width was 69.85 mm, and its thickness was 3.175 mm. The beam was equipped with four M-8557-P1 Macro Fiber Composite piezoelectric patches [13] in a collocated configuration [14, 15]. Two were placed 3 mm from the left clamped edge and two were placed at 35 mm from the right edge. The images in Fig. 2 show the structure and its components. The actuators were powered by a PA05039 TREK High Voltage Power Amplifier. The beam was excited at a point 10 mm from the top edge and 20 mm from the right clamped edge with a Brüel & Kjaer electrodynamic vibration exciter. The force delivered was monitored by a Brüel & Kjaer force transducer, with a sensitivity of 0.5 mN in conjunction with a Brüel & Kjaer 2692-C Nexus charge amplifier. The beam's displacement was measured using a OFV-505 Polytec Laser Doppler Vibrometer with an LMS SCADAS III front-end data acquisition system. Two positions along the beam were measured, to obtain data for the first and second mode. The mode 1 measurement point was located at the center of the beam, at 258.5 mm from the clamped end. The mode 2 measurement point was located at a quarter of the beam length, at 129.25 mm from the edge. These positions were chosen to best capture the motion of the specific modes, based on their mode shapes. The first and second modes shapes of the beam are given in Fig. 3.

During the nonlinear testing of the beam, a harmonic step-sine excitation was delivered to the beam at 5 forcing levels, ranging from 0.5 N to 3 N, over two frequency ranges, one of 55 Hz to 77 Hz and the other of 150 Hz to 167 Hz. These ranges were chosen to surround the first and second modes. The step resolution was 0.5 Hz, with a 20-cycle delay between steps. The previously presented control algorithm was designed in SIMULINK and loaded onto a dSpace DS1103 PPC Controller Board.

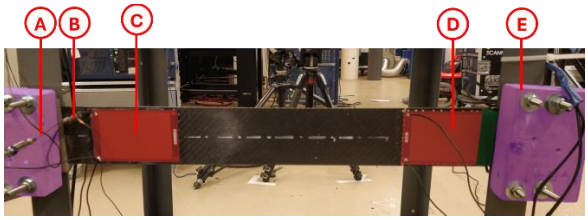

(a)

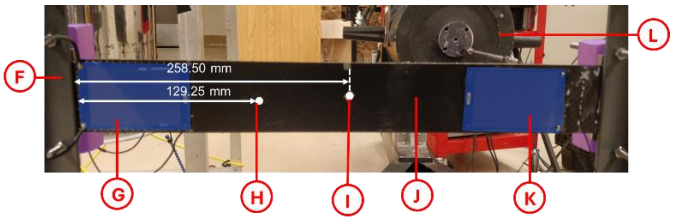

(b)

Figure 2. Diagram of the experimental set-up of the clamped beam with dimensions and details. (a) Back (excitation side); (b) Front (measurement side). A: Stinger; B: Force transducer; C: Actuator 1; D: Actuator 2; E: Clamp; F: Metal frame; G: Sensor 2; H: Mode 2 measurement point; I: Mode 1 measurement point; J: Composite beam; J: Sensor 1; L: Exciter.

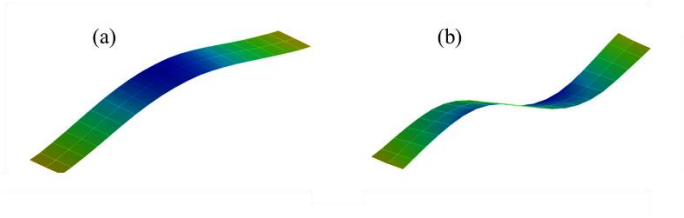

Figure 3. First two natural modes of the beam. (a) Mode 1; (b) Mode 2.

IV. RESULTS

The purpose of this study was to assess the effectiveness of a nonlinear dual-mode MIMO controller in reducing the amplitude of vibration of the first 2 modes of nonlinear vibration of a sandwich beam. The effects of nonlinearity as well as the MIMO configuration and dual-mode architecture were assessed as well. The vibration attenuation produced by each controller was analyzed using the following equation,

$$R = 100\% \cdot \left| \frac{z_{uncontrolled} - z_{controlled}}{z_{uncontrolled}} \right|, \qquad (6)$$

which calculates the percent reduction in the maximum vibration amplitude as compared to the uncontrolled case.

A. *Nonlinear dual-mode MIMO controller results*

The effects of the nonlinear dual-mode MIMO controller on the vibration amplitude of the beam were tested and the resulting frequency response curves for each forcing level are given in Fig. 4, as compared to the uncontrolled case. The reduction percentage compared to the uncontrolled case was calculated using (6), and the results are presented in Table II. Furthermore, the actuation voltages required to implement this controller were measured. The maximum actuation voltage differential was obtained for each actuator at each different forcing level and plotted in a bar chart for modes 1 and 2. This plot is shown in Fig. 5. The actuation voltage differential defines the difference between the maximum and minimum voltages required throughout the actuator usage. Since the manufacturer specifications for the actuator patches require the actuation voltage to remain between +1500 and -500 V, the maximum actuation voltage differential acceptable is 2000 V.

TABLE II. PERCENT AMPLITUDE REDUCTION OBTAINED FOR EACH FOCRING LEVEL WITH THE NONLINEAR DUA-LMODE MIMO CONTROLLER.

Forcing level (N)	Reduction (%)	
	Mode 1	Mode 2
0.5	81.9	54.3
1	82.4	60.2
1.5	84.0	60.0
2	86.3	62.1
3	85.6	65.3

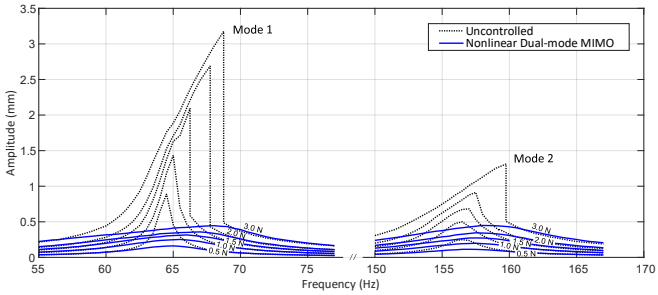

Figure 4. Nonlinear vibration amplitude curves for forcing levels of 0.5 N to 3.0 N for the uncontrolled beam (black dotted) and the beam controlled by the nonlinear dual-mode MIMO controller (blue).

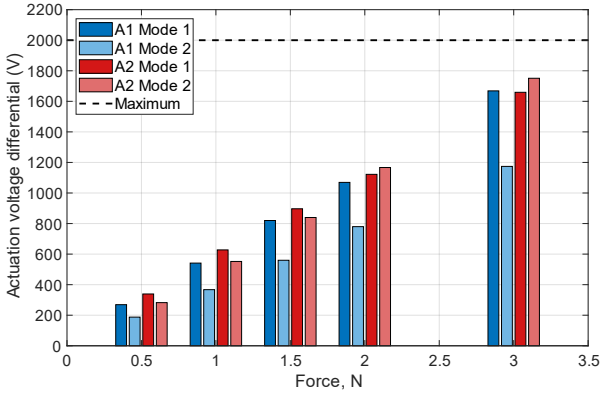

Figure 5. Maximum actutation voltage differentials per forcing level for actuators 1 (blue) and 2 (red), modes 1 (dark) and 2 (pale), for the beam controlled by a nonlinear dual-mode MIMO controller. The dotted line indicates the maximum acceptable voltage differential accodring to the hardware manufacturer.

B. *Nonlinear vs linear control*

The effects the nonlinear term were investigated by comparing the nonlinear dual-mode MIMO controller to a linear dual-mode MIMO controller. For this controller, all parameters were kept the same except the nonlinear stiffness term η_{f_3}, which was set to 0 for both modes. The results of this controller's effects on the vibration amplitude are shown in the frequency response curves for forcing levels from 0.5 N to 3 N in Fig. 6. Here, the nonlinear dual-mode MIMO (blue) is compared to the linear dual-mode MIMO (red), and to the uncontrolled case (black). The maximum actuation voltage differentials of the linear dual-mode MIMO controller are presented in Fig. 7. From these figures and from Table III, which gives the percentage of reduction for each forcing level as calculated using (6), it is evident that the nonlinear term improves control over the first mode by 5% for lower forcing levels to 10% for higher ones. The nonlinear term does not, however, make a big difference for mode 2, where reductions remain within 2-3% of each other from one controller to the next. The actuation voltage differential plots show higher voltage differentials for the nonlinear controller, which is expected.

TABLE III. PERCENT AMPLITUDE REDUCTION OBTAINED FOR EACH FOCRING LEVEL WITH THE LINEAR DUAL-MODE MIMO CONTROLLER.

Forcing level (N)	**Reduction (%)**	
	Mode 1	**Mode 2**
0.5	78.3	53.8
1	76.1	60.2
1.5	76.2	57.8
2	78.2	59.4
3	76.0	60.1

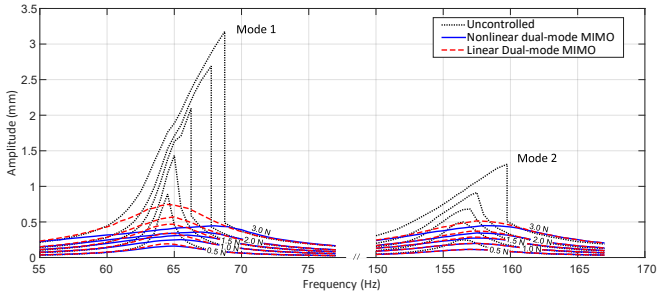

Figure 6. Nonlinear vibration amplitude curves for forcing levels of 0.5 N to 3.0 N for the uncontrolled beam (black dotted) and the beam controlled by the nonlinear dual-mode MIMO controller (blue) and the beam controlled by the linear dual-mode MIMO controller (red dashed).

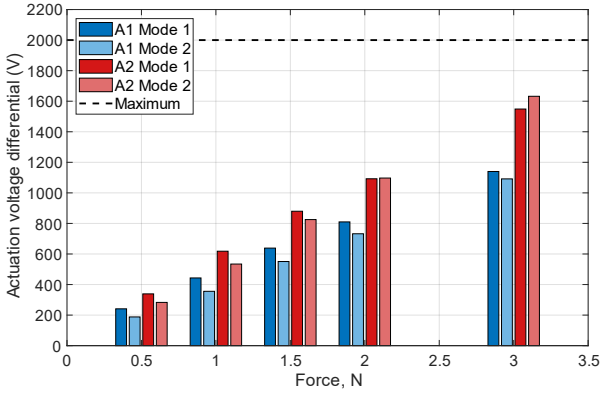

Figure 7. Maximum actutation voltage differentials per forcing level for actuators 1 (blue) and 2 (red), modes 1 (dark) and 2 (pale), for the beam controlled by a linear dual-mode MIMO controller. The dotted line indicates the maximum acceptable voltage differential accodring to the hardware manufacturer.

C. *SISO vs MIMO control*

The effects of the MIMO architecture were investigated by comparing the dual-mode MIMO controller to a dual-mode SISO controller. Only actuator 2 and sensor 2 were used for this controller and the resulting $\boldsymbol{B}_{\boldsymbol{a}}^{*}$ and $\boldsymbol{C}_{\boldsymbol{s}}^{*}$ matrices were then $\boldsymbol{B}_{\boldsymbol{a}}^{*} = \begin{bmatrix} 0 \\ 1 \end{bmatrix}$ and $\boldsymbol{C}_{\boldsymbol{s}}^{*} = [0 \quad 1]$ for both modes 1 and 2. Fig. 8 shows the results of this controller's effects while Fig. 9 presents its maximum voltage differentials. Notably, the actuator 1 voltage differentials are all 0, as this actuator was not in use. Table IV also gives the percent amplitude reduction observed at each forcing level, as calculated using (6) again. From these plots and this table, it can be seen that the percent amplitude reduction is improved by 5% to 10% by the MIMO controller for mode 1, but by almost 50% for mode 2. The MIMO controller is therefore significantly better at controlling mode 2 than the SISO.

TABLE IV. PERCENT AMPLITUDE REDUCTION OBTAINED FOR EACH FOCRING LEVEL WITH THE DUAL-MODE SISO CONTROLLER.

Forcing level (N)	**Reduction (%)**	
	Mode 1	**Mode 2**
0.5	76.4	9.24
1	74.1	14.1
1.5	74.7	9.37
2	77.8	10.9
3	74.6	11.6

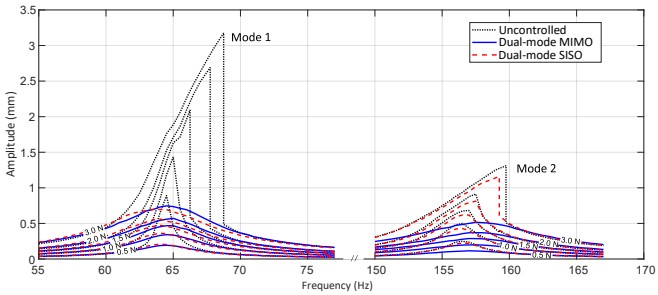

Figure 8. Nonlinear vibration amplitude curves for forcing levels of 0.5 N to 3.0 N for the uncontrolled beam (black dotted) and the beam controlled by the dual-mode MIMO controller (blue) and the beam controlled by the dual-mode SISO controller (red dashed).

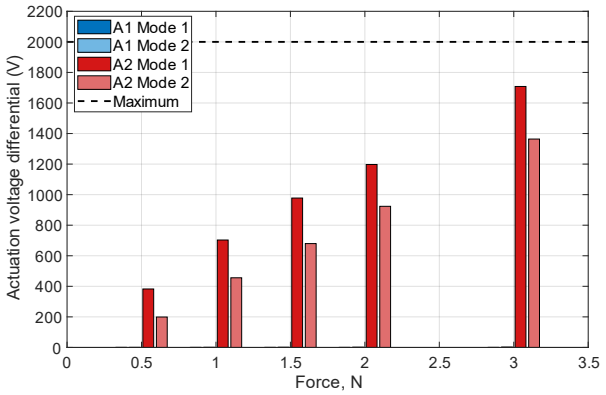

Figure 9. Effects Maximum actutation voltage differentials per forcing level for actuators 1 (blue) and 2 (red), modes 1 (dark) and 2 (pale), for the beam controlled by a dual-mode SISO controller. The dotted line indicates the maximum acceptable voltage differential accodring to the hardware manufacturer.

D. Dual-mode vs single-mode control

The effects of the dual-mode architecture were compared to two single-mode architectures, one targeting mode 1 and the other targeting mode 2. In each case, the parameters listed for the specified mode in Table 1 were used. The resulting frequency response curves are presented in Fig. 10, (a) and (b), with each case being compared to the uncontrolled beam and the dual-mode controller. The amplitude reduction percentages were calculated using (6) and presented in Table V (A) and (B), for the mode-1 and mode-2 targeted controllers respectively. Lastly, the maximum actuation voltage differentials were plotted in Fig. 11 (a) and (b) for the two controllers. We observe that the dual-mode controller performs similarly to the mode-1 targeted controller on mode 1, but that on mode 2, this controller has no effect, as seen by its near-zero actuation voltages on this mode. The mode-2 targeted controller works well on mode 2, as expected, but less well on mode 1.

TABLE V. (A) PERCENT AMPLITUDE REDUCTION OBTAINED FOR EACH FOCRING LEVEL WITH THE MODE-1 TARGETTED MIMO CONTROLLER.

Forcing level (N)	**Reduction (%)**	
	Mode 1	**Mode 2**
0.5	73.9	0.67
1.5	71.4	-0.85
2	73.1	1.87
3	69.7	3.73

(B) PERCENT AMPLITUDE REDUCTION OBTAINED FOR EACH FOCRING LEVEL WITH THE MODE-2 TARGETTED MIMO CONTROLLER.

Forcing level (N)	**Reduction (%)**	
	Mode 1	**Mode 2**
0.5	46.5	53.3
1.5	49.7	57.7
2	52.1	59.6
3	45.7	59.9

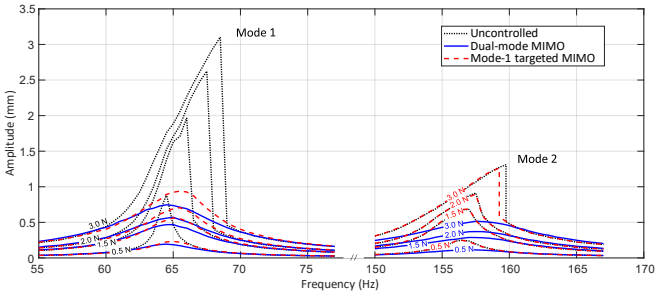

(a)

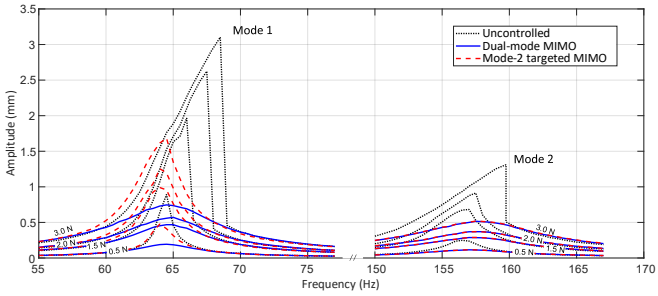

(b)

Figure 10. Nonlinear vibration amplitude curves for forcing levels of 0.5 N to 3.0 N for the uncontrolled beam (black dotted) , the beam controlled by the dual-mode MIMO controller (blue) and the beam controlled by the single-mode targed MIMO controllers (red dashed). (a): Mode-1 targetted; (b): Mode-2 targetted.

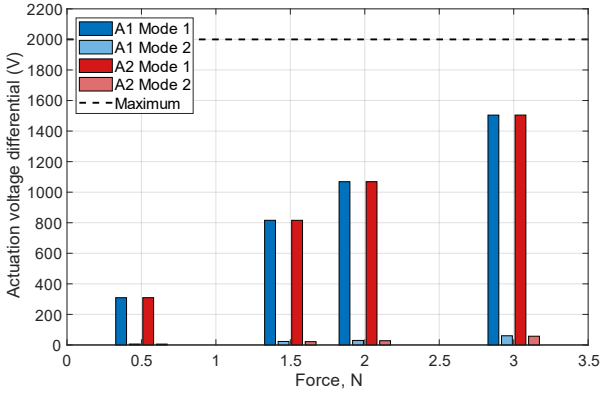

(a)

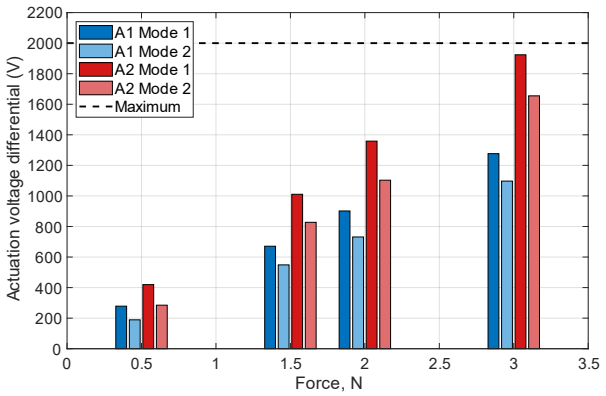

(b)

Figure 11. Effects Maximum actutation voltage differentials per forcing level for actuators 1 (blue) and 2 (red), modes 1 (dark) and 2 (pale), for the beam controlled by a single-mode MIMO controllers. The dotted line indicates the maximum acceptable voltage differential accodring to the hardware manufacturer. (a): Mode-1 targetted; (b): Mode-2 targetted.

V. Conclusion

The purpose of this study was to examine the effectiveness of using a nonlinear dual-mode MIMO controller in controlling the first 2 modes of vibration of a nonlinear hardening beam structure. The controller was compared to four other controllers: a linear dual-mode MIMO controller, a dual-mode SISO controller and two single-mode MIMO controllers, targeting modes 1 and 2 respectively. These comparisons established the effects of including the nonlinear term in the novel controller, and the importance of the both the MIMO architecture and the dual-mode targeting scheme. The maximum actuation voltage differentials were also presented in the form of bar charts, to ensure that the maximum voltages of the hardware were not exceeded. The nonlinear dual-mode MIMO controller was shown to outperform all four other controllers in the vibration reduction over both first and second modes of vibration of the beam, achieving a maximum reduction of 86% for mode 2 and 65% on mode 2. Maximum actuation voltage differentials reached a peak near 1800 V for this controller, which was greater than most other controllers, except for the mode-2 targeted MIMO, which presented a maximum actuation voltage differential of almost 2000 V.

Acknowledgment

The authors acknowledge the partial financial support of the NSERC Discovery and CFI-LOF grants of Canada, as well as of the talent program of the city of Hangzhou, Zhejiang province, China.

References

[1] A. H. Nayfeh, D. T. Mook, *Nonlinear oscillations*. John Wiley & Sons, 2008.

[2] S. Le Guisquet, M. Amabili, "Identification by means of a genetic algorithm of nonlinear damping and stiffness of continuous structures subjected to large-amplitude vibrations. Part I: single-degree-of-freedom responses," *Mechanical Systems and Signal Processing*, vol. 153, p. 107470, 2021.

[3] J. Delannoy, "Parametric Identification of Geometric Non-linearities of Mechanical Systems," M.E., McGill University (Canada), Canada -- Quebec, CA, 28250757, 2016.

[4] M. Amabili, *Nonlinear Vibrations and Stability of Shells and Plates*. Cambridge University Press, 2008.

[5] J. Ro and A. Baz, "Control of sound radiation from a plate into an acoustic cavity using active constrained layer damping," *Smart Materials and Structures*, vol. 8, no. 3, p. 292, 1999/06/01 1999, doi: 10.1088/0964-1726/8/3/302.

[6] C. J. Goh, T. K. Caughey, "On the stability problem caused by finite actuator dynamics in the collocated control of large space structures," *International Journal of Control*, vol. 41, no. 3, pp. 787-802, 1985/03/01 1985, doi: 10.1080/0020718508961163.

[7] J. L. Fanson, T. K. Caughey, "Positive position feedback control for large space structures," *AIAA Journal*, vol. 28, no. 4, pp. 717-724, 1990, doi: 10.2514/3.10451.

[8] M. I. Friswell, D. J. Inman, R. W. Rietz, "Active Damping of Thermally Induced Vibrations," *Journal of Intelligent Material Systems and Structures*, vol. 8, no. 8, pp. 678-685, 1997, doi: 10.1177/1045389x9700800805.

[9] S. N. Mahmoodi, M. Ahmadian, "Active Vibration Control With Modified Positive Position Feedback," *Journal of Dynamic Systems, Measurement, and Control*, vol. 131, no. 4, 2009, doi: 10.1115/1.3089565.

[10] G. Zhao, A. Paknejad, G. Raze, A. Deraemaeker, G. Kerschen, C. Collette, "Nonlinear positive position feedback control for mitigation of nonlinear vibrations," *Mechanical Systems and Signal Processing*, vol. 132, pp. 457-470, 2019.

[11] C. Hameury, G. Ferrari, G. Franchini, M. Amabili, "An experimental approach to multi-input multi-output nonlinear active vibration control of a clamped sandwich beam," *Mechanical Systems and Signal Processing*, vol. 216, 111496, 2024. doi: https://doi.org/10.1016/j.ymssp.2024.111496.

[12] C. Hameury, G. Ferrari, and M. Amabili, "A nonlinear dual-mode active vibration controller for hardening systems and its experimental application to a beam," *Journal of Sound and Vibration*, vol. 597, p. 118823, 2025, doi: https://doi.org/10.1016/j.jsv.2024.118823.

[13] SmartMaterial. MFC Engineering Properties. https://www.smart-material.com/MFC-product-propertiesV2.html

[14] A. Preumont, K. Seto, *Active control of structures*. John Wiley & Sons, 2008.

[15] M. K. Kwak, S. Heo, "Active vibration control of smart grid structure by multiinput and multioutput positive position feedback controller," *Journal of Sound and Vibration*, vol. 304, no. 1, pp. 230-245, 2007/07/10/ 2007, doi: https://doi.org/10.1016/j.jsv.2007.02.021.